Acta Cryst A FOUNDATIONS ADVANCES

ISSN 2053-2733

Chiral spiral cyclic twins

Wolfgang Hornfeck*

Institute of Physics of the Academy of Sciences of the Czech Republic, Na Slovance 2, 182 21 Praha 8, Czech Republic.
*Correspondence e-mail: hornfeck@fzu.cz

Received 14 July 2021
Accepted 17 November 2021

Edited by M. I. Aroyo, Universidad del País Vasco, Spain

Keywords: chiral; spiral; cyclic twins.

A formula is presented for the generation of chiral m-fold multiply twinned two-dimensional point sets of even twin modulus $m > 6$ from an integer inclination sequence; in particular, it is discussed for the first three non-degenerate cases $m = 8, 10, 12$, which share a connection to the aperiodic crystallography of axial quasicrystals exhibiting octagonal, decagonal and dodecagonal long-range orientational order and symmetry.

1. Introduction

The binary intermetallic compound NiZr exhibits a remarkable tendency of forming cyclic tenfold twins from either a vitrified amorphous matrix upon heating (Jiang *et al.*, 1985) or a deeply undercooled melt upon solidification (Hornfeck *et al.*, 2014, 2018).

Similar distinctive cyclic twinning phenomena occur in other intermetallic alloys, too, a particularly pronounced example being $Al_{20}Cu_2Mn_3$ (Feng *et al.*, 2014; Wang *et al.*, 2016). In nature, cyclic twins are commonly found in rutile-type structures, such as in the mineral cassiterite (SnO_2), as has been studied recently both in the context of the reticular theory of twinning (Nespolo & Souvignier, 2015), as well as in electron backscatter diffraction (EBSD) experiments performed on synthetic samples doped with CoO and Nb_2O_5 (Padrón-Navarta *et al.*, 2020). A geometric theory of cyclic growth twins (Ericksen, 2006) has been applied not only to multiple twins of rutile (TiO_2), but also to those found in aragonite ($CaCO_3$), marcasite (FeS_2) and quartz (SiO_2). The concept of cyclic twinning or cyclic intergrowth plays an important role in the description and classification of inorganic crystal structures (Hyde *et al.*, 1979; Andersson & Hyde, 1982; Andersson & Stenberg, 1982; Stenberg & Andersson, 1982; Andersson, 1983; Hyde & Andersson, 1989), with twinning phenomena in general, due to their variety and profundity, arguably forming their own subfield of crystallography: geminography (Grimmer & Nespolo, 2006).

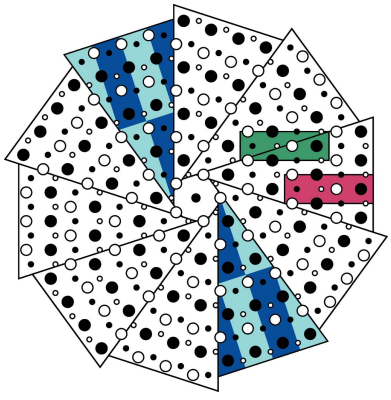

In order to better understand the twin formation process an atomistic model was developed (Hornfeck *et al.*, 2014, 2018; Hornfeck, 2018), based on some idealized geometric properties of NiZr's orthorhombic unit cell, including not only its special axial ratio, in the form of $2\tan^{-1}(a/b) \simeq 36^\circ$, being the prerequisite of tenfold twinning, but also taking into account special values for the atomic coordinates, governed by a $\mathbb{Z}$ module. This model has been experimentally confirmed at atomic resolution (Hornfeck *et al.*, 2018) by means of high-angle annular dark-field scanning transmission electron microscopy (HAADF-STEM), thereby making NiZr the first example of $\mathbb{Z}$-module twinning (Quiquandon *et al.*, 2016; Sirindil *et al.*, 2017, 2018). The atomistic model found (Fig. 1) exhibits some remarkable properties: (i) the structure in the

bulk of the twin domains is identical to the structure extending across the twin boundaries; (ii) the structure is chiral, featuring an irrational shift between adjacent twin domains; (iii) the structure is solely determined by the choice of the twin modulus, $m = 10$, determining a corresponding $\mathbb{Z}$ module (apart from a global scaling factor fixing the minimal interatomic distance); (iv) the structure features a unique description based on the union of ten spirals.

The latter point deserves particular attention. One important aspect to note about spiral patterns is their ubiquitous occurrence in nature [see Hammer (2016) for an excellent overview], in particular as growth forms in the plant and animal kingdoms, yet also in the form of screw dislocation based growth spirals (helices), in the inanimate realm of crystals. Spiral microstructures have been observed in some eutectic alloys as well (Fullman & Wood, 1954). Astonishing geometric regularity can thus be found in biology as well as chemistry, such as in the spatial arrangement of seeds in the sunflower floret (Vogel, 1979), as a specific example of phyllotaxis (Jean, 1995; Adler *et al.*, 1997; Pennybacker *et al.*, 2015), or the atoms in polymeric chain molecules (Müller, 2017), in which their spiral arrangement extends along a common screw axis into that of closely related three-dimensional helices, with the double-helical structure of DNA arguably the most important representative (Watson & Crick, 1953). In the field of crystallography botanical phyllotaxis inspired the study of spiral lattices (Rivier, 1988; Rothen & Koch, 1989*a*,*b*; Kunz & Rothen, 1992; Sadoc *et al.*, 2012), a concept pioneered and greatly expanded upon by Bursill and coworkers, both in direct and reciprocal space, and with relations to aperiodic crystals (Bursill *et al.*, 1987; Fan, Peng *et al.*, 1988; Fan, Bursill *et al.*, 1988; Bursill, 1990).

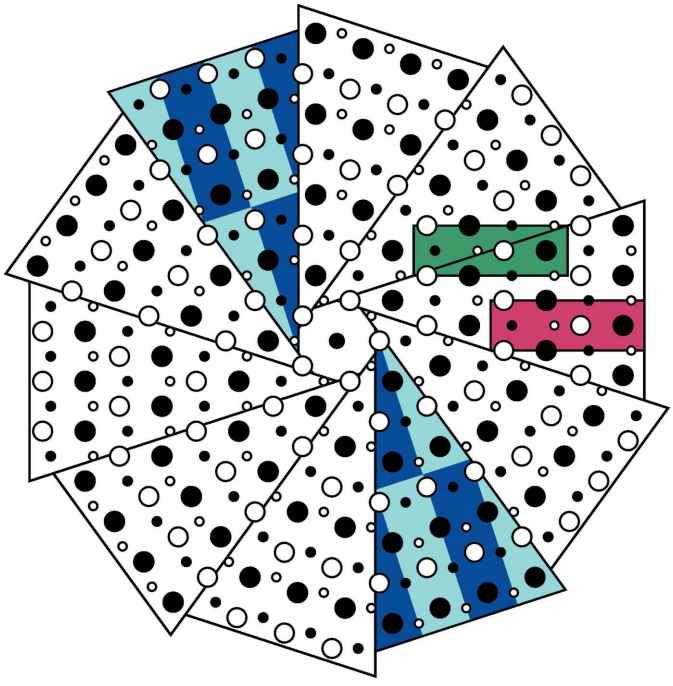

Figure 1
Idealized cyclic tenfold twin structure of NiZr. Distinct atom types and heights in the out-of-plane direction are highlighted by different circle styles and radii (Ni: solid circles; Zr: open circles; $z = 1/4$: small circles; $z = 3/4$: large circles). Highlighted by lines are the twin boundaries of ten wedge-like twin domains, shifted against each other in the way of an iris aperture, as well as two unit cells, one within the bulk of a twin domain (red) and one across a twin boundary (green). Note the chiral arrangement of twin domains, and the spiral arrangement of atoms, alternating both in atom type and height, thereby inducing a kind of antisymmetry between adjacent twin domains, reducing the symmetry from tenfold for the non-decorated two-dimensional twin to fivefold for the decorated three-dimensional one. Note also that in the twin only five distinct orientation states occur, with opposite domains (alternating blue/cyan unit-cell pattern) belonging to the same state.

For most of these examples, the geometric properties of a particular spiral type (Archimedean, logarithmic *etc.*) frequently match in a natural fashion with simple growth principles (equidistant layering, self-similarity/scale invariance *etc.*), thereby rationalizing the self-organization of matter on its way from chaos to order. By their observed morphology and microstructure, and following a simple geometrical argument, the formation of cyclic twins is naturally thought to originate in the nucleation from a single common seed. Yet, how exactly the twinning, which can be seen as a disadvantageous defect occurring in an otherwise undistorted bulk crystal, is induced first, and furthermore preserved during crystal growth, is much less clear (Shahani & Voorhees, 2016). In the case of NiZr, however, the spiral description suggests an intrinsic mechanism, in the form of a lateral growth program, explaining effortlessly the formation of a cyclically twinned microstructure and its spatial continuation into a macroscopically observable twinned morphology. The resulting twin structure is a highly correlated arrangement of atoms, and due to its perfect twin boundaries matching the bulk crystal, energetically favorable.

These favorable properties recommend an investigation into the potential of transcending the NiZr model into one of chiral spiral cyclic twins (CSCTs) of arbitrary *m*.

2. Exposition

The key to the desired generalization is given by exploring and exploiting the most suitable parametrization of the CSCT in order to prepare the stage for subsequent generalizations. In the following we state the obtained results and refer the interested reader to the extensive appendix containing a never-dared-to-ask-for discussion about the derivation and further optimization of this parametrization.

2.1. Parametrization

Two-dimensional CSCT point patterns can be parametrized by three numbers: (i) an integer modulus m, (ii) an integer multiplier μ_m and (iii) a real scaling factor τ_m. To cut things extremely short for the moment, the parametrization is based upon the use of the complex mth roots of unity

$$\omega_m^k = \exp(\mathrm{i}2\pi k/m) \tag{1}$$

and their combination according to

$$\Omega_{k,\ell} = \tau_m \omega_m^k + \sum_{j=0}^{\ell-1} \omega_m^{\kappa(j)+k} \tag{2}$$

with Cartesian coordinates resulting as points

$$P_{k,\ell} = (\mathrm{Re}\,\Omega_{k,\ell}, \mathrm{Im}\,\Omega_{k,\ell}) \tag{3}$$

suitably indexed as the ℓth spiral node of the kth spiral branch. Here,

$$\kappa(j) = \beta(j) + \{j - \beta(j)\} \bmod 2 \tag{4}$$

denotes an integer inclination function, itself described by an integer baseline function determined by the rule

$$\beta_\mu(j) \Rightarrow \text{the digit } j \text{ appears } 2\lfloor j/\mu_m \rfloor + 1 \text{ times}, \tag{5}$$

which, for the cases under discussion hereafter, can be expressed algebraically as

$$\beta(j) = \lfloor (\mu_m j)^{1/2} \rfloor. \tag{6}$$

Here, $\{\cdot\} \bmod \cdot$ and $\lfloor \cdot \rfloor$ denote the integer modulo and floor function, respectively. More details are given in the appendix.

Empirically it is found that only certain combinations of parameters yield a meaningful, uniformly distributed point pattern composed of self-avoiding discrete spirals. Noteworthy are the following triples (m, μ_m, τ_m), which will be discussed in detail hereafter: $(6, 1, 1)$, $[8, 1, 1 + (2)^{1/2}]$, $(10, 2, \tau)$ and $[12, 2, 1 + (3)^{1/2}]$. Here, $\tau = [1 + (5)^{1/2}]/2$ denotes the golden ratio. The triples with $m = 8, 10, 12$ are especially interesting because their rotational symmetry matches those of octagonal, decagonal and dodecagonal axial quasicrystals.

2.2. The case $m = 6$

As a prelude we briefly discuss the case $m = 6$. As it turns out, this is a degenerate case, not matching the subsequently described twin structures for $m = 8, 10, 12$, yet still of some interest in terms of its crystallographic interpretation. The sixfold 'chiral' spiral 'twin' is the hexagonal honeycomb grid (Fig. 2).

Thus, for indistinguishable points in an infinite pattern, it is neither chiral, nor a twin, since there are no observable boundaries, which would induce both properties to the point pattern. Instead, the hexagonal honeycomb grid is the vertex set of one of the three tessellations of the plane by regular convex polygons, with the other two tilings being based on the vertex set as defined by the two-dimensional triangular and square lattice.

The case $m = 6$ is also interesting, insofar as a cyclic twin nucleation has been reported to occur in tin-based solder alloys (Lehman *et al.*, 2010), which strongly resembles the cyclic twin nucleation phenomena observed for NiZr (Hornfeck *et al.*, 2018), yet differs in that the symmetry of the twin is sixfold.

2.3. The cases $m = 8, 10, 12$

The exploration of the parameter space (m, μ_m, τ_m), with the already known case $(10, 2, 1.618)$, and following the rationale described in the appendix, leads to the discovery of a regular CSCT described by the parameter triple $(8, 1, 2.414)$ with $\tau_8 = 1 + (2)^{1/2}$. This seemed to suggest a correspondence

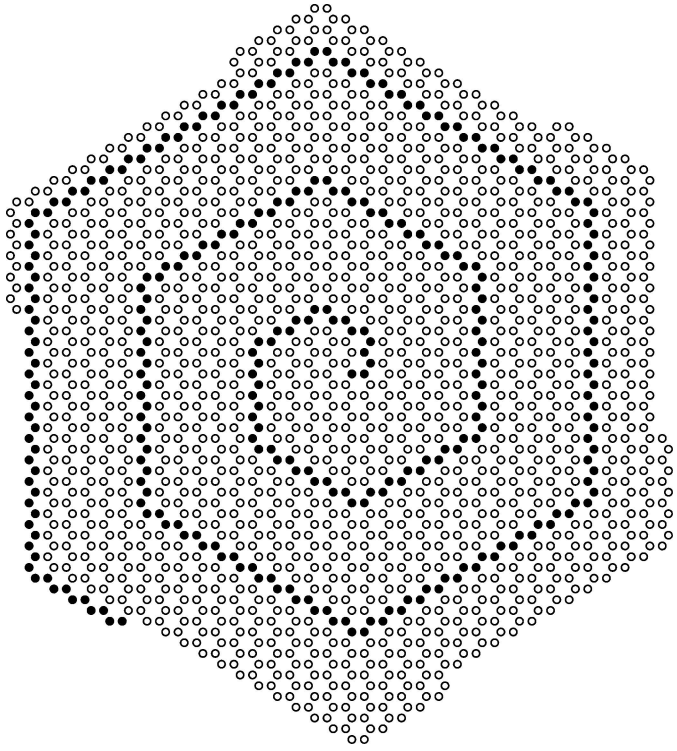

Figure 2
Sixfold CSCT (degenerate case). Shown are 300 points per spiral branch, 1800 in total. A single spiral branch is highlighted by solid circles.

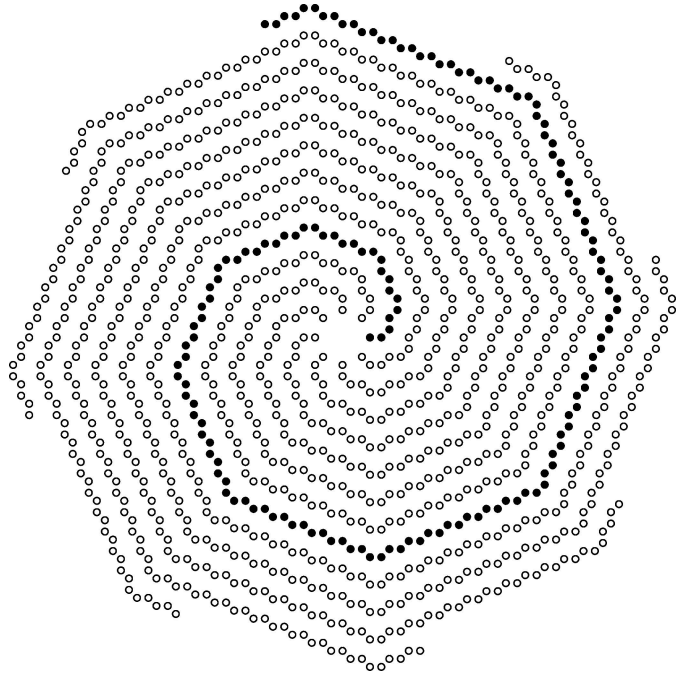

Figure 3
Eightfold CSCT. Shown are 150 points per spiral branch, 1200 in total. A single spiral branch is highlighted by solid circles.

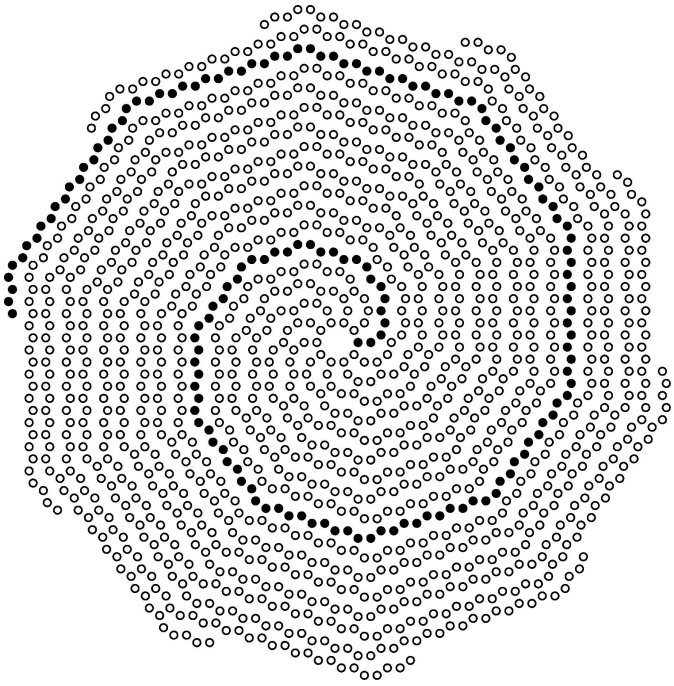

Figure 4
Tenfold CSCT. Shown are 150 points per spiral branch, 1500 in total. A single spiral branch is highlighted by solid circles.

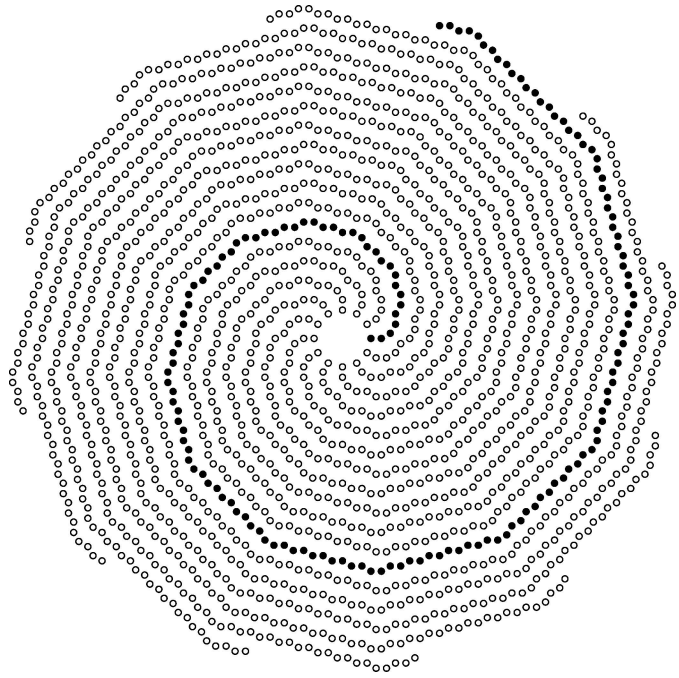

Figure 5
12-fold CSCT. Shown are 150 points per spiral branch, 1800 in total. A single spiral branch is highlighted by solid circles.

with the well known (Niizeki, 1989; Burdik *et al.*, 1998) and experimentally observed quadratic irrational inflation factors (see the appendix for the concept and notation)

$$\begin{aligned}\tau_8^{\rm IM} &= (1, 1, 2, 1) \simeq 2.414,\\ \tau_{10}^{\rm IM} &= (1, 1, 5, 2) \simeq 1.618,\\ \tau_{12}^{\rm IM} &= (2, 1, 3, 1) \simeq 3.732\end{aligned} \tag{7}$$

for intermetallic (IM) axial quasicrystals with eight-, ten- and 12-fold rotational symmetry, including the silver, golden and platinum ratio, respectively. Thus, a triple $(12, 3, 3.732)$ was checked for, yet did not yield a CSCT. Neither did a triple $(12, 3, 0.822)$ obtained by a linear extrapolation of the established octagonal and decagonal parameters, although its regularity was higher than in the aforementioned case. Instead, it was found empirically that the triple $(12, 2, 2.732)$ with $\mu_m = 2$ and $\tau_{12} = 1 + (3)^{1/2}$ yields a perfect solution! Figs. 3, 4 and 5 show the corresponding point patterns.

Notably, the observed factors $\tau_8 = 1 + (2)^{1/2}$ and $\tau_{12} = 1 + (3)^{1/2}$ can be associated with a single formula,

$$\tau_m = 1 + 2\cos(2\pi/m), \tag{8}$$

which is known to describe the inflation factors of certain quasiperiodic rhombic tilings of octagonal and dodecagonal symmetry as obtained by the projection method (Steurer & Deloudi, 2009; p. 38 for the octagonal Ammann–Beenker tiling and p. 40 for the dodecagonal rhomb tiling). Note that the inflation factor $\tau_{12} = 1 + (3)^{1/2}$, while not to be regarded the most characteristic inflation factor for dodecagonal tilings, occurs in several distinct instances (Schaad & Stampfli, 2021; see also https://geometricolor.wordpress.com/2012/07/29/another-tiling-of-dodecagonal-symmetry/ and https://geometricolor.wordpress.com/2021/03/04/yet-another-tiling-with-12-fold-rotational-symmetry/).

Now, equation (8) has a simple geometric interpretation as the circumcircle radius $R_{\rm CC}$ of the corresponding regular m-gon (Fig. 6), spanned by m triples of mutually adjacent thin and thick rhombs of unit edge length $e = 1$ [compare this with equation (58) in the appendix, in which the unit edge length $E = 1$ refers to the regular m-gon instead].

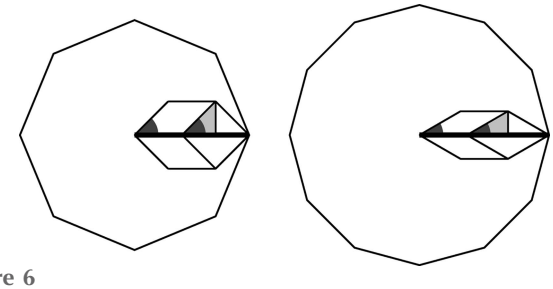

Figure 6
Derivation of the factor τ_m for the cases of $m = 8$ (left) and $m = 12$ (right). Shown are the central polygons of the CSCTs together with a triple of mutually adjacent rhombs. The triple is composed of a pair of thin rhombs oriented towards the center and a single thick rhomb at the periphery. The thin rhombs have an acute angle of $\alpha = 2\pi/m$ (dark gray), which corresponds to half of the acute angle of a single thick rhomb, which, in the special case of $m = 8$, corresponds to half of a right angle of a square. A right triangle (light gray) can be constructed and used to determine the length of a segment of the circumcircle radius (thick line) of the polygon to be equal to $e\cos\alpha$, in which e denotes the edge length of a rhomb. Then, the total circumcircle radius is equal to $R = e + 2e\cos\alpha$, and for e set to unity, $\tau_m = 1 + 2\cos\alpha$ follows.

Table 1
Parameters for m-fold CSCTs.

Analytical expressions are given where known as well as the minimal polynomials of which τ_m is a root. For the meaning of the indices i, j see equation (14).

m	μ_m	τ_m (numerical)	τ_m (analytical)	Minimal polynomial	i	j
6	1	1.000 000	1	1	1	3
8	1	2.414 214	$1+(2)^{1/2}$	x^2-2x-1	3	8
10	2	1.618 034	$[1+(5)^{1/2}]/2$	x^2-x-1	2	5
12	2	2.732 051	$1+(3)^{1/2}$	x^2-2x-2	3	12
14	3	2.246 980		x^3-2x^2-x+1	3	7
16	3	2.847 759	$1+[2+(2)^{1/2}]^{1/2}$	$x^4-4x^3+2x^2+4x-1$	3	16
18	4	2.879 385		x^3-3x^2+1	4	9
20	4	2.902 113	$1+[5/2+(5)^{1/2}/2]^{1/2}$	$x^4-4x^3+x^2+6x+1$	3	20
22	5	3.513 337		$x^5-3x^4-3x^3+4x^2+x-1$	5	11
24	5	2.931 852	$1+[2+(3)^{1/2}]^{1/2}$	$x^4-4x^3+2x^2+4x-2$	3	24

2.4. The general scheme

Thus, from the small number of observations made so far, and taking the approach detailed in the appendix into account, one might boldly generalize the existence of two series of CSCTs, one for $m = 6, 10, 14, 18, 22, \ldots$ and another one for $m = 8, 12, 16, 20, 24, \ldots$. In particular, if $m' = m/2$ is an odd number, one obtains (see the appendix)

$$\mu_m = (m-2)/4 \quad \text{and} \quad \tau_m = \frac{1}{2\sin(\pi/m)}, \tag{9}$$

while one obtains

$$\mu_m = (m-4)/4 \quad \text{and} \quad \tau_m = 1+2\cos(2\pi/m), \tag{10}$$

for m' being an even number. By using the alternating functions

$$S = (-1)^{m'} \quad \text{and} \quad M = \{m'\} \bmod 2 \tag{11}$$

in which $m' > 3$, one can combine both parameter evolutions into a single set

$$\mu_m = (m - 2^{2-M})/4 = \lfloor (m'-1)/2 \rfloor, \tag{12}$$

$$\tau_m = \left[1 - M + 2\cos\left(\frac{2-Mm}{2^M m}\pi\right)\right]^S \tag{13}$$

of formulas, which inherently include the case distinctions.

Eventually, it is observed that all scaling factors τ_m also follow an alternative formula, common for both series,

$$\tau_m = \Delta(i,j) = \frac{\sin(i\,\pi/j)}{\sin(\pi/j)}, \tag{14}$$

in which $\Delta(i,j)$ denotes the ith out of the $\lfloor j/2 \rfloor$ distinct diagonals of a regular j-gon of unit edge length $E = \Delta(1,j) = 1$ (Fontaine & Hurley, 2006; *cf.* Fig. 7). Here, the observed value of j follows the splitting pattern for m' being an odd or even number, with $j = m/2^M$, whereas the value of i shows an individual pattern alternating between a linear increase for the odd cases and a constant one for the even ones. The parameters for the CSCTs up to $m = 24$ have been collected for easy reference in Table 1.

As a summary, any given triple fully characterizes a CSCT, with each parameter on its own determining certain of its geometrical features: (i) the modulus $m \in \mathbb{N}$, denoting the order of the rotation axis, determines the number of twin domains and the successive angular inclinations of the spiral branches. (The number of distinct orientation states, the twin multiplicity, is only half as big, since opposite domains share the same orientation state, see Fig. 1.) (ii) The multiplier $\mu_m \in \mathbb{N}$ determines the location of the inclination points occurring on a spiral branch, by controlling the repeat number of alternating steps occurring in-between the inclination points. (iii) The multiplier $\tau_m \in \mathbb{R}$ defines the circumcircle radius R_{CC} of the innermost m-gon, in relation to the unit moduli along the spiral, together forming a pair $(\tau_m, 1)$ of multipliers.

3. Discussion

After showing how the CSCTs are generated, a conceptualization of what has been found is given in the following discussion, highlighting the CSCTs' relation to Archimedean spirals and circle involutes, as well as $\mathbb{Z}$ modules.

3.1. Archimedean spiral and circle involute description

Although the spirals used for the description of the CSCTs are discrete in nature, they can be approximated by continuous curves, which is of particular interest for a more comprehensive characterization of CSCTs in terms of their general geometric properties and their large-scale asymptotic behavior. While a direct interpolation by some general curve is always possible, it is never unique, thereby limiting deeper insights (Davis, 1993; p. 34). Instead, it is rather more important to note the type of continuous spiral, some common examples of which are given by Bursill *et al.* (1987), that will represent a best fit to the discrete set of spiral nodes $P_{0,\ell}$. The most common types of spirals, often known since antiquity, are usually fully described by very few parameters only, thus being ideal candidates for the aforementioned purpose. A number of textbooks have compiled information about spirals and other curves, their construction, properties and applications (Eagles, 1885; Lockwood, 1961; Zwikker, 1963; Lawrence, 1972; Yates, 1974; Shikin, 1995; Rutter, 2000).

Now, the layer-by-layer growth of the discrete spiral gives the crucial clue for the unique type of continuous spiral featuring a constant separation distance between successive turns, thereby ruling out a kind of spiral similarity symmetry in the sense of Shubnikov (1961). In fact, two closely related candidates exist, namely the Archimedean spiral and the involute of a circle. In the case of the Archimedean spiral a constant separation distance between consecutive convolutions is observed along rays radiating from its origin, but with the caveat that the intersections of these rays with the spiral are not perpendicular. For the involute of the

circle, however, a constant separation distance is measured along common normals of consecutive convolutions of the curve.

Despite this subtle yet important difference, both curves are intimately related to one another, and thus can be treated within a general system of parametric equations, suitably formulated in matrix-vector form

$$\begin{bmatrix} x(s,t) \\ y(s,t) \end{bmatrix} = R\, \mathcal{T}_{ab}(s,t) \begin{bmatrix} \cos t \\ \sin t \end{bmatrix}, \tag{15}$$

in which R is a common scalar reference radius, and the matrix is defined as

$$\mathcal{T}_{ab}(s,t) = \begin{bmatrix} a & b(t-s) \\ -b(t-s) & a \end{bmatrix}, \tag{16}$$

with the choice of matrix parameters a, b discriminating the cases

$$\begin{aligned} \mathcal{T}_{10}(s,t) &= \text{circle}, \\ \mathcal{T}_{01}(s,t) &= \text{Archimedean spiral}, \\ \mathcal{T}_{11}(s,t) &= \text{circle involute}. \end{aligned} \tag{17}$$

Here, the additional fixed parameter $s \in [0, 2\pi]$ designates a single spiral's starting point in terms of a cyclic phase shift. In particular, the value $s = 0 = 2\pi$ represents the starting points $(0, 0)$ and $(R, 0)$ for the Archimedean spiral and the involute of the circle, respectively, for the parameter $t = 0$. For spirals starting at phase angles $s \neq 0$ the parameter t starts from a shifted starting point, $t = s$, as well.

In a dynamic perspective an Archimedean spiral is defined as the locus of a point that moves away from another, fixed point at uniform linear velocity v (radially) and uniform angular velocity ω (azimuthally). As a consequence of the described uniform motion, Archimedean spirals feature a constant separation distance of $2\pi R$.

In order to obtain the best fit curve, it is actually better to use a polar plot of a point's radius vector length r versus its polar angle θ, yielding the simple linear function

$$r(\theta) = R\theta + s \tag{18}$$

in which the slope $R = v/\omega$ is given as the quotient of the radial and azimuthal velocities, and in which the ordinate intercept s is related to the starting point $(s, 0) = (R\pi/2, 0)$. Since a point in our chosen parametrization is represented by a complex number, both the radius and the angle have a simple representation as a point's complex absolute value and absolute argument, respectively.

Polar plots for the CSCTs with $m = 8, 10, 12$ are shown in Fig. 7 together with their approximations with

$$R_8 = 2.916,\ R_{10} = 2.368 \text{ and } R_{12} = 3.481 \tag{19}$$

determined by a simple linear least-squares procedure (*Mathematica*).

Note that while the slopes increase in the unnatural order $m = 10, 8, 12$, this matches the ascending order of their scaling factors $\tau_{10} \simeq 1.618$, $\tau_8 \simeq 2.414$ and $\tau_{12} \simeq 2.732$, respectively.

A plot of the CSCT for the case $m = 8$ is shown in Fig. 8 together with its circle of radius $R = R_8$, circle involutes for $s = n2\pi/8\,(n = 0, \ldots, 7)$ and Archimedean spiral for $s = 0$.

Note that the above parametrization has been chosen so as to account for a fixed phase shift $p = -\pi/2$ between the

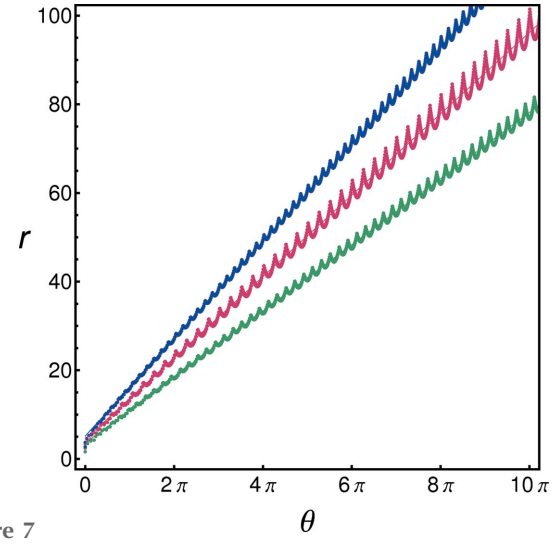

Figure 7
Polar plot r versus θ (in radians) for the spirals of modulus $m = 8$ (red, middle), $m = 10$ (green, bottom) and $m = 12$ (blue, top). Note the observed simple proportionality $r \propto \theta$ (overall, approximate) characteristic for an Archimedean spiral. Note, also, the broken order in terms of the value of the slope, with the curve for $m = 10$ featuring the smallest value, thereby indicating a non-unique rule for the spiral's generation.

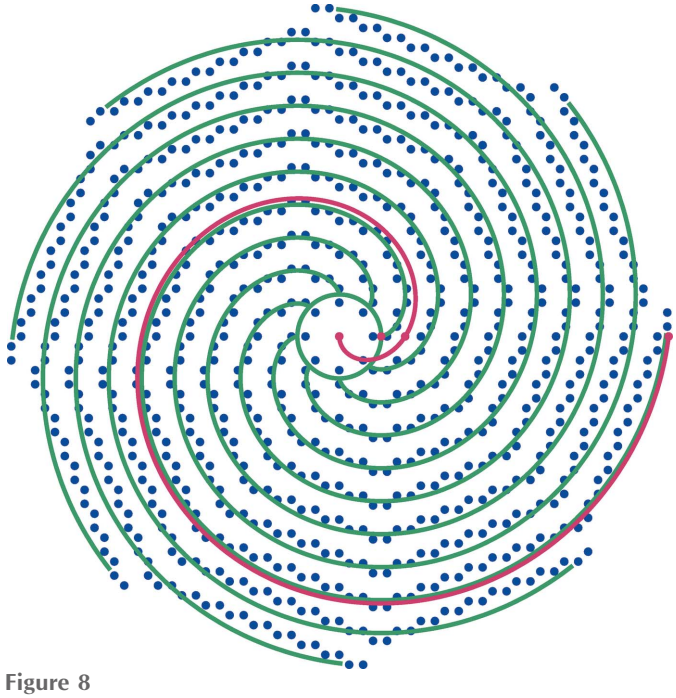

Figure 8
Discrete spiral pattern of an eightfold CSCT (800 points; blue) together with its continuous approximation by eight circle involutes (green) and one Archimedean spiral (red). Highlighted points (red) on the real number line are the origin, $(0, 0)$, as well as the points $(R, 0)$, $(R\pi/2, 0)$ and $(R\pi/2 + 2\pi R, 0)$ in which R denotes the circle radius $(R = R_8 \simeq 2.996)$.

circle involute and the Archimedean spiral, such that any given pair of a circle involute and its corresponding Archimedean spiral can be associated with the same variable phase shift s, thereby highlighting their asymptotic equivalence for $t \to \infty$.

3.2. $\mathbb{Z}$-module description

For a single spiral branch, each node's position in the complex plane is, by definition, a linear combination of unit basis vectors represented by a complex summation over the roots of unity. By this means a single spiral branch traces a path in what is known by mathematicians as a $\mathbb{Z}$ module, a higher-dimensional generalization of a lattice (Steurer & Deloudi, 2009, p. 61; Sirindil *et al.*, 2017). In particular, a $\mathbb{Z}$ module of rank n, existing in a vector space $\mathbb{R}^d$ of dimension $d \leq n$, can be described by the set of points

$$\{z_1\mathbf{e}_1 + z_2\mathbf{e}_2 + \ldots + z_n\mathbf{e}_n | z_1, z_2, \ldots, z_n \in \mathbb{Z}\} \qquad (20)$$

which form an integer lattice $\mathbb{Z}^n$, spanned by n linear independent basis vectors $\mathbf{e}_i$, in the n-dimensional vector space $\mathbb{R}^n$. For $d = n$ this describes the special case of a lattice, while for $d < n$ this corresponds to the projection of a higher-dimensional lattice in n dimensions into the $\mathbb{Z}$ module in d dimensions.

Now, the generation of the full CSCT structure demands the additional complex multiplication with all possible roots of unity ω_m^k, which leads to the question of whether this relation to a $\mathbb{Z}$ module still holds true for the CSCT as a whole, despite the occurrence of the central radius vectors $\tau_m\omega_m^k$ of length $\tau_m > 1$ in the parametrization. While it is conjectured to hold true for general m, for the most interesting cases $m = 8, 10, 12$ this question can be answered in the affirmative, with a visual proof given in Fig. 9. Here, the proof consists of finding a continuous path, solely constructed of unit length segments, connecting the origin P_{00} of a single spiral branch with the origin $(0, 0)$ of the CSCT, and thus, by the action of the m-fold rotational symmetry, connecting all spiral branches with each other.

This relation to a $\mathbb{Z}$ module implies that every point on a single spiral branch, with in our case $d = 2$ real coordinates, can be indexed (in real space) instead by n integers z_i, where $n = 4$ for the octagonal, decagonal and dodecagonal cases. Apart from the formalism this means that the CSCT structures are exceptionally highly correlated structures, in which every position is precisely in registry with the underlying $\mathbb{Z}$ module. The $\mathbb{Z}$-module description thus highlights a hidden algebraic order among the coordinates with the presented parametrization by a single formula acting as a quantitative crystal structure descriptor (Hornfeck, 2012).

Moreover, since all points of the octagonal, decagonal and dodecagonal CSCTs are located on a $\mathbb{Z}$ module, we expect a possible description of these patterns by means of a higher-dimensional cut-and-project scheme, as well as their diffraction patterns to exhibit perfect octagonal, decagonal and dodecagonal symmetry, arising from the long-range orientational order present in the point patterns, similar to the crystallography of quasicrystals. Thus, the CSCTs with $m = 8, 10, 12$, while not being quasicrystals themselves (and experimentally discernible from them by the diffraction of a single domain), share a common characteristic of this special class of aperiodic crystals. Indeed, they are role models for the twins proposed by Pauling in his argument against the existence of quasicrystals.

4. Conclusion

A theoretical study has been made on chiral spiral cyclic twins with an emphasis on twins of eightfold, tenfold and 12-fold symmetry generated by the application of a unique integer-valued inclination function in a parametrization based on complex roots of unity. The underlying association of each generated point pattern's coordinates with those represented by a $\mathbb{Z}$ module highlights the highly correlated nature of this spatial arrangement, illustrates the importance of hidden algebraic relations presenting a form of symmetry going beyond the group-theoretical one, and establishes a connection to the crystallography of octagonal, decagonal and dodecagonal axial quasicrystals, respectively.

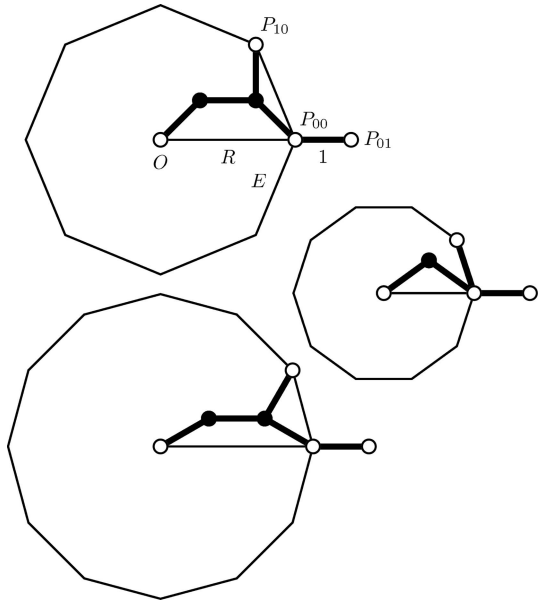

Figure 9
Geometry of the central polygon for the octagonal, decagonal and dodecagonal twin shown top left, middle right and bottom left, respectively. Highlighted in each case as open circles are the origin O as well as the points P_{00}, P_{10} and P_{01}, whose relative location (in the graph-theoretical sense) is the same for all depicted cases, as is the absolute distance of unity between the points P_{00} and P_{01}. The circumcircle radii R and edge lengths E differ, however. Note that in the decagonal case the edge length equals the distance between the points P_{00} and P_{01}, and that the circumcircle radii correspond to the respective scaling factors, $R = \tau_m$. Points highlighted as solid circles depict unit distance connections between adjacent spiral branches and to the origin, with their rotationally equivalent points omitted for clarity. Unit distance lines are shown with greater thickness.

APPENDIX A
Modeling of chiral spiral cyclic twins

In the following a detailed description of the derivation of the fundamental formula modeling CSCT structures is given, with each section discussing specific details of the modeling process.

A1. Two-dimensional model

For the parametrization the focus is laid on a purely two-dimensional point pattern, acting as an abstract model for the CSCT structure of NiZr as illustrated in Fig. 1, and obtained from it by a projection of the structure along the tenfold axis.

This is possible, because the tenfold twin structure of NiZr is essentially a (2+1)-dimensional structure, with the cyclic twinning occurring in the plane perpendicular to the tenfold axis, along which the three-dimensional twin structure is periodic.

This is similar to the case of axial quasicrystals, in which the quasiperiodicity also is restricted to a two-dimensional subspace.

Indeed, a periodicity in the twin plane is only observed within and strictly limited to any of the ten single twin domains, while the infinite pattern as a whole is aperiodic. Its symmetry is restricted to a point group composed of pure rotations, singling out the origin as a fixed point and implying the point pattern's chirality. The pattern's chirality is reflected in a spiral arrangement of atoms, akin to the phyllotactic arrangement of seeds in a sunflower floret, except for the presence of spirals of one handedness only.

The parametrization can take advantage of the abstract model's two-dimensional nature by the use of complex coordinates, in particular using the tenth roots of unity ω, defined by $\omega^{10} = 1$, as basis vectors. Anticipating the general case of an m-fold twin pattern, a general mth root of unity is given by the complex number, written in exponential form,

$$\omega_m^k = \exp(\mathrm{i}2\pi k/m), \tag{21}$$

in which k runs from zero to $m-1$ in order to produce all distinct roots.

Exponential sums of the general form

$$S(n) = \sum_{j=1}^{n} \omega_1^{f(j)}, \tag{22}$$

in which $f(j)$ is a real-valued function defined on the positive integers, show a rich variety of geometric forms, including spiral ones, in plots of all their partial sums up to the given n (Lehmer & Lehmer, 1979, 1980; Loxton, 1983; Deshouilliers, 1985; Chamizo & Raboso, 2015). Sums of the aforementioned type are commonly referred to by the name of Weyl sums, as they feature prominently in the study of uniform distribution modulo one, as pioneered by Hermann Weyl (Dekking & Mendèz France, 1981).

In our case, each point located on a single spiral branch of a CSCT is parametrized by the complex number

$$\Omega_{0,\ell} = \tau_m \omega_m^0 + \sum_{j=0}^{\ell-1} \omega_m^{\kappa(j)}, \tag{23}$$

obtained by adding the individual contributions of the mth roots of unity in a consecutive manner. Here, $\kappa(j)$ is a non-negative-integer-valued inclination function (see below). The full m-fold point pattern is generated from a single spiral branch's points by multiplying the $\Omega_{0,\ell}$ with the appropriate complex mth root of unity:

$$\Omega_{k,\ell} = \omega_m^k \Omega_{0,\ell} = \tau_m \omega_m^k + \sum_{j=0}^{\ell-1} \omega_m^{\kappa(j)+k}. \tag{24}$$

Here, k and ℓ denote spiral coordinate indices, designating the ℓth spiral node on the kth spiral branch.

Cartesian coordinates (x, y) are obtained as the real and imaginary parts of the complex number $\Omega_{k,\ell}$, namely as the two-dimensional point $P_{k,\ell} = (\mathrm{Re}\,\Omega_{k,\ell}, \mathrm{Im}\,\Omega_{k,\ell})$. Note that $P_{0,0}$ is *not* denoting the origin, but the point $(\tau_m, 0)$.

The real number τ_m denotes a fixed scaling factor, in particular $\tau(\mathrm{NiZr}) = \tau_{10} = [1 + (5)^{1/2}]/2$ is the golden ratio, and is chosen such that the distance between consecutive spiral nodes is unity, including, in the case of NiZr, the edge length of the central m-gon. Apart from an arbitrary general scaling factor, not stated explicitly, this choice fixes the model.

Finally, the mirror-symmetric twin of opposite chirality is obtained by replacing every instance of a complex root of unity by its complex conjugate counterpart. Here, a plus (minus) sign in the exponent corresponds to a counter-clockwise (clockwise) oriented, right-handed (left-handed) spiral, following the usual convention (Fan, Peng *et al.*, 1988).

A2. Three-dimensional model

In a realistic three-dimensional model further scaling factors have to be taken into account, following NiZr's orthorhombic unit-cell metrics (Hornfeck, 2018). In addition, atom types (Ni or Zr) and atom heights (1/4 or 3/4) in the c direction have to be specified. This can be done as a function of the two-dimensional spiral coordinates k and ℓ as

$$\mathrm{atom}(\ell) = \begin{cases} \mathrm{Ni} & \text{for } \ell \bmod 2 = 0 \\ \mathrm{Zr} & \text{otherwise} \end{cases} \tag{25}$$

$$z(k, \ell) = \frac{1}{2} + \frac{(-1)^{\{k+\ell\} \bmod 2}}{4}. \tag{26}$$

Notably, the assignment of alternating atomic heights, apart from creating a two-layer structure, reduces the tenfold symmetry to a fivefold one. Thus, alternating twin domains appear flipped, in accordance, however, with a relative shift of atomic positions by $z = 1/2$. As is the case for axial quasicrystals, the structure can be continued periodically in the c direction.

A3. Inclination function as a binary case distinction

The inclination function $\kappa(j)$ of equation (23) encodes all the information about the consecutive coordinate evolution tracing out a given spiral branch k up to a given spiral node ℓ for a specific CSCT. For the case of NiZr it was empirically found (Hornfeck, 2018) to be defined as

$$\kappa(j) = \left\{\left\lfloor [2(j-1)]^{1/2} \right\rfloor + [j \in \mathcal{J}]\right\} \bmod 10 = \left\{\beta(j) + \alpha(j)\right\} \bmod 10, \quad (27)$$

with

$$\mathcal{J} = \left\{\left\lceil 2[n + (n)^{1/2}] \right\rceil \mid n \in \mathbb{N}\right\} = \{4, 7, 10, 12, \ldots\}. \quad (28)$$

Here, $\lceil\cdot\rceil$, $\lfloor\cdot\rfloor$ and $\{\cdot\} \bmod \cdot$ are the integer-yielding ceiling, floor and modulo functions, respectively, while

$$[C] = \begin{cases} 1 & \text{if } C \text{ is true,} \\ 0 & \text{otherwise,} \end{cases} \quad (29)$$

denotes the Iverson bracket, checking its argument C is true or false, thus forming a generalization of an indicator function [see Graham *et al.* (1994) for the definition and properties of all integer functions]. In the case of equation (27), the condition to check for is given by the question of set membership of the variable j in the set $\mathcal{J}$. The use of the Iverson bracket allows for an alternative definition of the complex number

$$\Omega_{k,\ell} = \tau_m \omega_m^k + \sum_{i=0}^{m-1} \sum_{j=0}^{\ell-1} [i = \kappa(j)] \omega_m^{i+k}, \quad (30)$$

in the way that the summation of the complex unit vectors is not carried out on a consecutive basis, as in equation (23), but instead by counting the total number of occurrences of a given ith root of unity ω_m^i, out of m distinct ones, up to the number ℓ of nodes. Note that the modulo operation can be skipped for the application of $\kappa(j)$ in the exponent of a complex mth root of unity [*cf.* equation (23)], since these form a cyclic group, yet not in the condition of the Iverson bracket used in equation (30).

The two summands in equation (27) give rise to the following sequences:

$$\beta(j) \Rightarrow 0, 1, 2, 2, 2, 3, 3, 3, 4, 4, 4, 4, 4, 5, 5, 5, 5, 5, \ldots, \quad (31)$$

$$\alpha(j) \Rightarrow 0, 0, 0, 1, 0, 0, 1, 0, 0, 1, 0, 1, 0, 0, 1, 0, 1, 0, \ldots. \quad (32)$$

As can be seen from this comparison, the sequence $\beta(j)$ defines a baseline, increasing by one at certain steps of increasing interval length, while the sequence $\alpha(j)$ is alternating between the values of zero and one, in an intricate, yet certainly not irregular fashion.

Both sequences added (modulo 10) yield the spiral sequence

$$\kappa(j) \Rightarrow 0, 1, 2, 3, 2, 3, 4, 3, 4, 5, 4, 5, 4, 5, 6, 5, 6, 5, \ldots, \quad (33)$$

the numbers of which, ranging from zero to nine, specify one out of ten basis vector directions.

The twin model of NiZr was constructed by adhering to certain geometrical constraints imposed by NiZr's crystal structure (Hornfeck *et al.*, 2014). Its parametrization by the spiral sequence of equation (33) followed only afterwards (Hornfeck *et al.*, 2018; Hornfeck, 2018) and by empirically finding the suitable integer sequences for the baseline and alternating part in the *On-line Encyclopedia of Integer Sequences* (OEIS; Sloane, 2018). This has several drawbacks.

First, seen from a technical point of view, the construction of the alternating sequence could not be made in a *direct* way, *i.e.* the sequence $\alpha(j)$ of equation (32) could not be found in the OEIS, and accordingly no formula for its generation is yet known. Only by transforming its information, by stating the position of ones, and thereby forming another sequence, encoded in the set $\mathcal{J}$ of equation (28), can its description be allowed in an *indirect* way.

Second, any generating formula found faces the problem of being *non-unique* – usually several immediate alternatives exist, and, in principle, an infinitude of them. This is, of course, not a mathematical problem. The description of the spiral sequence by one formula or another mathematically equivalent one makes no practical difference whatsoever. However, the conceptual difference is huge, thinking in terms of explaining not *how* the formula works, but *why* it does. Without knowing this, there seem also no opportunities for obvious generalizations to other than tenfold symmetric cases.

A4. Inclination function as a binary constant

For the purpose of a more direct generation of the alternating sequence $\alpha(j)$ of equation (32), one idea is to identify it with a binary number by means of concatenating zeros and ones according to the set membership condition and in the order in which they appear in the sequence:

$$\theta_{10} = (0.000\,100\,100\,101\,001\,010\,\ldots)_2. \quad (34)$$

The knowledge of θ_{10} then allows for an alternative representation of the inclination function as

$$\kappa(j) = \left\{\left\lfloor [2(j-1)]^{1/2} \right\rfloor + \lfloor 10^j \theta_{10} \rfloor\right\} \bmod 10. \quad (35)$$

An analytic expression of the constant θ_{10} is given by the infinite reciprocal sum [*cf.* equation (28)]

$$\theta_b = \sum_{n=1}^{\infty} b^{-\lceil 2[n+(n)^{1/2}] \rceil}, \quad (36)$$

which, after a combination of manual and computer-assisted (*Mathematica*) algebraic transformations, evaluates to

$$\theta_b = \frac{(b+1) - (b-1)[b^{-1/2}\vartheta_2(b^{-2}) + \vartheta_3(b^{-2})]}{2(b^2-1)} \quad (37)$$

in the case of general base b. Here, $\vartheta_i(q)$ is a shorthand notation for Jacobi's second and third theta function,

$$\vartheta_2(z, q) = 2q^{1/4} \sum_{k=0}^{\infty} q^{k(k+1)} \cos[(2k+1)z], \quad (38)$$

$$\vartheta_3(z, q) = 1 + 2 \sum_{k=1}^{\infty} q^{k^2} \cos(2kz), \quad (39)$$

stated for the special case in which the complex argument z is equal to zero. The so-called nome q is restricted according to $|q| < 1$.

Jacobi theta functions are interrelated by numerous algebraic identities, and can be expressed in a multitude of infinite series and product representations, with a rich number-theoretic background. In particular, they appear in the closed-form expressions for similar constants, *e.g.* for the infinite sums

of reciprocals of the Fibonacci and Lucas numbers (Borwein & Borwein, 1987). With the complex argument z being zero, they also occur in the exact evaluation of lattice sums, of which the Madelung constant is the most prominent example (Borwein *et al.*, 2013; Zucker, 2017).

However, the aforementioned approach is still not well suited for generalization, since for each case it requires the derivation of another specific constant.

A5. Inclination function as a binary string

In order to generate the alternating sequence $\alpha(j)$ of equation (32) in a more direct way, we analyze the pattern of zeros and ones of which the sequence is made. For this purpose we switch to a representation of the sequence by a string by concatenating zeros and ones, just as we did for the representation as a binary number, yet skipping the leading zero and decimal point. Now, the baseline sequence [equation (31)] suggests a *splitting pattern* according to 0|0|010|010|01010|01010|0..., due to the incremental change of digits and with respect to the interval lengths in between. A comparison with equation (31) shows that we have the following multiplicities times digits: 1×0, 1×1, 3×2, 3×3, 5×4, 5×5, and so on. The multiplicities run over the odd integers, yet with a period of two, which could be highlighted by introducing a second marker | at the appropriate positions: 0|0||010|010||01010|01010||0.... Obviously the pattern between the markers is very simple – just the alternation of zeros and ones – with ever-increasing odd number interval lengths while one proceeds along the string. In the limit of an infinite string this would result in a periodic alternation of zeros and ones, ...01..., which could be thought of the average string underlying the inclination pattern. In a plot this would just correspond to a rectified 'spiral', so any of the observed differences are really caused by the occasionally interspersed additional steps preferring one direction over the other, thereby creating a true spiral and a chiral twin structure. Now, the average sequence is generated by

$$\langle\alpha(j)\rangle = (j \bmod 2)_{j=0}^{\infty} \tag{40}$$

and it is clear that the need to adjust the sequence, in such a way that the alternating sequence $\alpha(j)$ is recovered, is connected to the incremental increase of the baseline sequence $\beta(j)$, in particular to the positions when an incremental step occurs. In these cases the average sequence has to be shifted/extended by one bit, thereby creating the intermittant ...00... repeats. Taking these arguments into account one finds

$$\alpha(j) = \{j - \beta(j)\} \bmod 2 \tag{41}$$

as the correct function. Here, the baseline generating function

$$\beta(j) = \lfloor (2j)^{1/2} \rfloor \tag{42}$$

was adjusted for an offset of one, in order to let the sequence start with an index j of zero, as is the case for the average sequence $\langle\alpha(j)\rangle$. With this we have

$$\kappa(j) = \{\beta(j) + \{j - \beta(j)\} \bmod 2\} \bmod 10, \tag{43}$$

where j starts from zero. This formula has the advantage of using only simple integer functions, while effectively coupling the alternating sequence to the baseline one. As such it can be very simply generalized to

$$\begin{aligned}\kappa_\mu(j) &= \{\beta_\mu(j) + \{j - \beta_\mu(j)\} \bmod 2\} \bmod m \\ &= \left\{ j - 2\left\lfloor \frac{j-\beta_\mu(j)}{2} \right\rfloor \right\} \bmod m \end{aligned} \tag{44}$$

with the general baseline function

$$\beta_\mu(j) = \lfloor (\mu j)^{1/2} \rfloor \tag{45}$$

and two fixed parameters, a multiplier μ and a modulus m.

A6. Properties of the generalized alternating function $\alpha_\mu(j)$

In order to see why

$$\alpha_\mu(j) = \{j - \beta_\mu(j)\} \bmod 2 \tag{46}$$

gives a *uniquely* alternating sequence of zeros and ones, as a function of $\beta_\mu(j)$, let us use the identity $x \bmod n = x - n\lfloor x/n \rfloor$ and thus

$$\alpha_\mu(j) = j - \beta_\mu(j) - 2\left\lfloor \frac{j-\beta_\mu(j)}{2} \right\rfloor. \tag{47}$$

Since both j and $\beta_\mu(j)$ are integers by definition [*cf.* equation (45)] we can include each of them separately into one of the two floor functions

$$-\left\lfloor \frac{j-\beta_\mu(j)}{2} - j \right\rfloor - \left\lfloor \frac{j-\beta_\mu(j)}{2} + \beta_\mu(j) \right\rfloor \tag{48}$$

and further simplify, by using the identity $-\lfloor -x \rfloor = \lceil x \rceil$, to

$$\left\lceil \frac{j+\beta_\mu(j)}{2} \right\rceil - \left\lfloor \frac{j+\beta_\mu(j)}{2} \right\rfloor. \tag{49}$$

It is now clear that $\lceil x \rceil - \lfloor x \rfloor$ can only assume the values of zero (if x is an integer) or one (otherwise), as implied by the modulo function of modulus two. For the argument $x = (1/2)[j + \beta_\mu(j)]$ to be distinct from an integer, the sum $j + \beta_\mu(j)$ of the integers j and $\beta_\mu(j)$ has to be odd, which is to say that either one of the summands has to be odd, while the other one has to be even. Since j runs consecutively over the integers, thereby alternating between odd and even values, the result will be one, whenever $\beta_\mu(j)$ fails to follow this alternation, which happens for every other value within the resulting baseline function's plateaus.

A7. Properties of the generalized baseline function $\beta_\mu(j)$

The core of the presented parametrization is given by the baseline function $\beta_\mu(j)$, which governs the path traced out by the spiral, in terms of its inclination points and their relative distance on the spiral arc. As such, this restricts its mathematical properties rather rigorously.

A function under consideration has to adhere to the following requirements. It has to map an integer input, the intermediate node index j, to an integer output, the intermediate baseline level, $\beta_\mu: \mathbb{Z} \to \mathbb{Z}$. In the presented baseline function $\beta_\mu(j)$ this is achieved by the floor function. Further-

more, the baseline levels have to start at zero and increase monotonically, so as to represent the increasing radial distance of a spiral node from the spiral's origin. The floor function guarantees a stepwise increase of the baseline levels, thereby yielding straight spiral segments within each twin domain [here, we refer to the spiral segments being *straight*, apart from the alternating pattern induced by the function $\alpha_\mu(j)$, which is disregarded for the sake of argument]. The increase of the baseline levels has to decrease with increasing intermediate node index j, since the farther apart a straight spiral segment is situated, the larger has to be its length, *i.e.* the relative distance between consecutive inclination points on the spiral.

Naturally, the combination of these requirements already rules out many of the fundamental mathematical functions, while the floored square root function $\lfloor(\mu j)^{1/2}\rfloor$ just happens to fulfill all of these requirements. This baseline function is a step function of increment one and plateaus constantly increasing in their length, due to the monotonously, yet ever more slowly increasing continuous function $(\mu j)^{1/2}$. The multiplier μ is a constant for any fixed m, but its functional dependence for varying m has yet to be clarified.

A8. Properties of the generalized baseline parameter μ

While the mathematical appearance of the baseline function $\beta_\mu(j)$ can be rationalized in a rather straightforward manner, a physical interpretation of the baseline parameter μ appears to be less evident. In order to get a feeling about its influence on the twin point pattern one can, however, study its extremal behavior in the limits $\mu \to 0$ and $\mu \to \infty$.

For the case $\mu \to 0$ one observes an ever-expanding length of the straight spiral segments until, at $\mu = 0$, the spiral branch is fully rectified. In this case the baseline function becomes zero everywhere, $\beta_\mu(j) = 0$, which means that the inclination and the alternating function become equal, $\kappa(j) = \alpha(j)$, resulting in a strictly alternating sequence, $\kappa(j) \Rightarrow 0, 1, 0, 1, 0, 1, \ldots$, of baseline level values. Upon increasing μ again a single spiral branch with a fixed number of nodes first gets more curled up, with its winding number around the origin increasing and its straight segment perpendicular separation distance decreasing accordingly. At some point, however, the regularity of the point pattern of a single spiral branch gets lost, since for $\mu \to \infty$ the inclination sequence defined by $\kappa(j)$ becomes more and more indistinguishable from a random sequence of baseline level values ranging between zero and $m-1$, with any given value occurring in the sequence with its natural uniform density $1/m$ for $\ell \to \infty$. A single spiral thus eventually transforms into a random walk about the origin. This behavior is known for the graphs of the partial sums of exponential sums in which the phase values of the summands are proportional to a square root function (Loxton, 1983; Chamizo & Raboso, 2015).

A9. Heuristics for the discovery of yet-unknown triples

Which triples (m, μ_m, τ_m) generate a CSCT? One way to answer this question would be an exhaustive search by applying a brute-force sampling of the parameter space. Since point patterns of already rather moderate modulus, say $m > 24$, are becoming less and less interesting, due to the diminishing size of individual twin domains, this task seems feasible. However, one does not know exactly which, maybe non-integer, values the multiplier μ_m might take, and since the multiplier τ_m is observed to be an irrational number, any search by an incremental variation of the parameters will anyhow only yield an approximate solution, which, in the best case, could result in an educated guess regarding the ideal value of this constant. If one assumes a variation of the parameters in the intervals $0 \le p \le 10^1$ by an incremental resolution of $(10^0, 10^{-3}, 10^{-3})$ this amounts to roughly 10^9 trial cases.

In practice, however, this approach failed not due to any computational intractability of the search itself, but due to a lack of algebraic methods for automatic checking of the geometric regularity of the candidate solutions. A check by visual inspection, although taking advantage of the supreme pattern recognition abilities of the human visual system, the eyes and the brain, proved to be utterly tedious, since the overwhelming number of trial cases turns out to be far away from being regular. At least there is a lesson learned here, too: any parameter triple, if it exists, has to be fine-tuned, since even the slightest deviations from the ideal parameter values quickly destroy the geometric regularity of the point pattern.

Instead of an exhaustive approach, a better way seems to be to find some heuristics for focusing the search on promising candidates. While the modulus m might simply be chosen to correspond to some of the known numbers $m = 8, 10, 12$ occurring for axial quasicrystals, a good guess for the other parameters is more difficult. However, since τ_{10} is the golden ratio, one might assume suitable candidates for other τ_m factors to be similar well known numbers, possibly occurring as members of some general number families.

For instance, the golden ratio occurs as the $\rho(1, 1)$-member of the family of infinite, nested radicals:

$$\rho(d, n) = \left\{ n + \left[n + (n + \ldots)^{1/(d+1)} \right]^{1/(d+1)} \right\}^{1/(d+1)} . \qquad (50)$$

On the other hand, the member $\rho(2, 1)$ is a constant known under the name plastic ratio, and both ratios are Pisot–Vijayaraghavan (PV) numbers, the plastic ratio also being the smallest such number. A PV number is a real algebraic integer α greater than unity, all of whose conjugate elements $\overline{\alpha}_i$ have absolute value less than unity (PV property): $\alpha > 1 > |\overline{\alpha}_i| > 0$. The PV property proves to be of particular importance in the theory of quasiperiodic substitution tilings in defining their self-similar inflation factors and other of their properties, and thus seems to be a good heuristic for which to check.

Like the golden ratio, the plastic ratio is an algebraic number, which means that it is a complex (real) root of a non-zero polynomial in one variable, with rational (integer) coefficients, where the polynomial is usually assumed to be of minimal degree. The minimal polynomial for the golden ratio is given by $x^2 - x - 1$ (of degree 2), while the one for the plastic ratio is given by $x^3 - x - 1$ (of degree 3). Being the root

of a minimal polynomial of degree two makes the golden ratio an algebraic number of degree two, and in particular a quadratic irrational number

$$(a, b, c, d) = \frac{a + b(c)^{1/2}}{d}, \tag{51}$$

in which a, b, c, d are integers, with b, c, d being non-zero and c being square-free. The property of being a quadratic (or cubic) irrational number was used to explain the occurrence of quasicrystals with m-fold rotational order only for $m = 5, 8, 10, 12$ (Levitov, 1988). The golden ratio corresponds to $(1, 1, 5, 2) \simeq 1.618$. The silver ratio, appearing as the self-similar inflation factor for the octagonal Ammann–Beenker quasiperiodic tiling, corresponds to $(1, 1, 2, 1) \simeq 2.414$. Both the golden and the silver ratio are part of a larger series of metallic ratios of the general form $(n, 1, n^2 + 4, 2)$, which are defined by their infinite continuous fraction representation of

$$n + \cfrac{1}{n + \cfrac{1}{n + \ddots}} = [n; n, n, \ldots] = \frac{n + (n^2 + 4)^{1/2}}{2}, \tag{52}$$

or by being a root of the quadratic equation $x^2 - n\,x - 1$, with $n = 1$ and $n = 2$ corresponding to the golden and silver ratio, respectively. The next, $n = 3$, member of the series, representing the bronze ratio $(3, 1, 13, 2) \simeq 3.303$ has also been associated with a two-dimensional quasicrystal, of hexagonal symmetry, formed in simulations of hard-core/square-shoulder colloidal particles (Dotera *et al.*, 2017; Nakakura *et al.*, 2019).

In general, the inflation factors of quasiperiodic tilings can be calculated from the tiling's substitution rules, which relate the number of tiles before and after an inflation step. The possibility of repeating an inflation step over and over again *ad infinitum*, from an aperiodic finite patch until its ultimate extension to the infinite plane itself, proves the quasiperiodicity of the tiling. The substitution rules can be formulated as a system of linear equations, with the number of individual tile multiplicities upon inflation forming a coefficient matrix. The eigenvalues of this coefficient matrix, being the roots of its characteristic (possibly minimal) polynomial, encode the information about the number of tiles after the nth inflation step, as well as the asymptotic proportions of tiles in the limit $n \to \infty$. In this limit only the largest root is dominant and thus defines the inflation factor.

Despite the general theory for self-similar inflation factors of quasiperiodic substitution tilings, it is actually not a trivial task to find the exact values for a given modulus m, for several reasons: (i) many more tilings are informally known than formally published, although there exists an extensive monograph (Grünbaum & Shephard, 1987) as well as promising attempts at an all-encompassing atlas of tilings (Frettlöh *et al.*, 2020); (ii) no coherent standard seems to exist in reporting the properties of tilings; (iii) existing results are scattered few and far between in a large body of literature; (iv) existing results are hard to search for, since synonymous expressions prevail, such as substitution factor, expansion factor, deflation factor or length expansion; (v) values for the inflation factor are not always stated explicitly.

For certain non-periodic rhombic substitution tilings with m-fold symmetry, however, Brown (2018) has described an easy and systematic way of obtaining the characteristic polynomials from Pascal's triangle (Fig. 10).

For this purpose the triangle is left-justified and sliced diagonally, with the integers within a slice forming the coefficients, alternating by their sign, of the sought-for polynomial. For instance, one obtains the following five first polynomials

$$\begin{aligned} P_6(x) &= x - 1 \\ P_{10}(x) &= x^2 - 3x + 1 \\ P_{14}(x) &= x^3 - 6x^2 + 5x - 1 \\ P_{18}(x) &= x^4 - 10x^3 + 15x^2 - 7x + 1 \\ P_{22}(x) &= x^5 - 15x^4 + 35x^3 - 28x^2 + 9x - 1 \end{aligned} \tag{53}$$

of general formula

$$P_m(x) = \sum_{i=0}^{\mu_m} (-1)^i \binom{\mu_m + i}{\mu_m - i} x^{\mu_m - i} \tag{54}$$

having only positive, real roots. The degree μ_m of the polynomial is related to the order m of the rotational symmetry of the twin pattern by $m = 4\mu_m + 2$. The scaling factor τ_m is given as the square root of the largest polynomial root, yielding

$$\begin{aligned} \tau_6 &= 1 \\ \tau_{10} &= 1.618\,033\ldots \\ \tau_{14} &= 2.246\,979\ldots \\ \tau_{18} &= 2.879\,385\ldots \\ \tau_{22} &= 3.513\,337\ldots. \end{aligned} \tag{55}$$

These scaling factors show a linear relationship with μ, which was estimated for the first 100 values to be equal to

$$\tau_m \simeq 0.636\,513\,\mu_m + 0.326\,681 \tag{56}$$

with a coefficient of determination R^2 almost equal to unity. This approximate linear relationship should facilitate an interpolation to the scaling factors of intermediate cases for which $m \neq 4\mu_m + 2$. Moreover, by using Plouffe's inverse

1										
1	1									
1	2	1								
1	3	3	1							
1	4	6	4	1						
1	5	10	10	5	1					
1	6	15	20	15	6	1				
1	7	21	35	35	21	7	1			
1	8	28	56	70	56	28	8	1		
1	9	36	84	126	126	84	36	9	1	
1	10	45	120	210	252	210	120	45	10	1

Figure 10
Left-justified Pascal's triangle with diagonals, some of them highlighted in distinct colors, used for the calculation of the scaling factor.

symbolic calculator (Plouffe, 1998), we find all these numbers to be equivalent to

$$\tau_m^{\mathrm{PT}} = \frac{\cos[\pi/m]}{\cos[(1/2)(m-4)(\pi/m)]} = \frac{1}{2\sin(\pi/m)}, \qquad (57)$$

thus establishing a relation between τ_m and m. Here, the superscript PT denotes the Pascal's triangle family of tilings. Since m was related to μ_m before, the triple of parameters needed to specify a cyclic twin has effectively reduced to the choice of a single parameter. This could be μ_m, as it is the natural index variable used in the construction before, or m since it corresponds to the order of the rotational symmetry of the cyclic twin under consideration. In any case the coupling of the model's parameters reduces any arbitrariness in the twin's construction.

Another aspect is remarkable. The formula found by inverse symbolic calculation and subsequent computer algebraic simplification is identical to the formula for the circumcircle radius

$$R_{\mathrm{CC}} = \frac{E}{2\sin(\pi/m)} \qquad (58)$$

of a regular m-gon of unit edge length $E = 1$. This relates the above series of scale multipliers τ_m to a simple property of the central polygon of the CSCT.

A drawback of the approach just presented is that it misses out on the interesting values of $m = 8, 12$. Thus, for these cases another solution had to be found empirically.

A10. Further refinement of the baseline function

The investigation of CSCTs with $m > 12$ is interesting as well, because quasicrystals with a corresponding higher m-fold symmetry, for instance $m = 18$ or $m = 24$, exist in soft condensed-matter systems (Dotera *et al.*, 2014). Some general trends can be inferred from plots of their point patterns (not shown). On the one hand, the overall appearance of the CSCTs, expressed by their convex hulls, becomes more and more indistinguishable from a circle, as is to be expected for a compounded point pattern consisting of regular polygons with an ever-increasing number of edges. Individual spiral branches progressively approximate circle involutes, due to both the straight spiral segments decreasing in their relative length and the alternating inclinations differing by a decreasing angle, respectively. As a consequence, the individual wedge-shaped twin domains, their facetting and boundaries, become less and less visually recognizable. On the other hand, the increasing baseline parameter value μ_m counteracts the emerging regularity, in that jumps of the baseline function become more frequent and their sequence more erratic. In summary, the point patterns appear less regular than those for the cases $m = 6, 8, 10, 12$. Eventually, the inclination pattern results in collisions, thus rendering the approach ultimately futile for both large m and ℓ, respectively. Indeed, it seems rather remarkable that the approach works perfectly for the cases $m = 6, 8, 10, 12$.

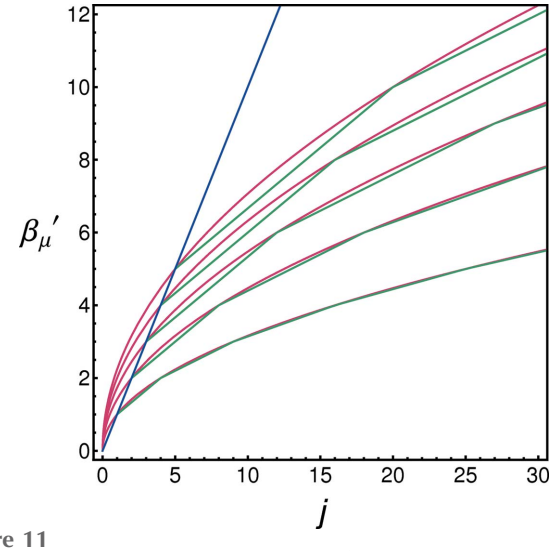

Figure 11
The first five square root functions $(\mu j)^{1/2}$ (red) with $\mu = 1, 2, 3, 4, 5$ (counted from below) and their piecewise linear approximations (green) shown together with the limiting line $\beta_\mu' = j$ (blue). The prime highlights that the plots depict the argument of the baseline function β_μ before performing the floor operation.

The lack of regularity can be attributed to a breakdown occurring in the spiral sequences going from

$$\begin{aligned}
&\beta_1(j) \Rightarrow 0, 1, 1, 1, 2, 2, 2, 2, 2, 3, 3, 3, 3, 3, 3, 3, 4, \ldots \\
&\beta_2(j) \Rightarrow 0, 1, 2, 2, 2, 3, 3, 3, 4, 4, 4, 4, 4, 5, 5, 5, 5, \ldots \\
&\beta_3(j) \Rightarrow 0, 1, 2, 3, 3, 3, 4, 4, 4, 5, 5, 5, 6, 6, 6, 6, 6, \ldots
\end{aligned} \qquad (59)$$

to

$$\beta_4(j) \Rightarrow 0, 2, 2, 3, 4, 4, 4, 5, 5, 6, 6, 6, 6, 7, 7, 7, 8, \ldots. \qquad (60)$$

While for $\beta_\mu(j)$, with $\mu = 1, 2, 3$ and starting at $j = 0$, the pattern can be described according to the rule stated in equation (5), this is not any longer true for $\beta_\mu(j)$ with $\mu \geq 4$. Replacing the function $\beta_\mu(j) = \lfloor (\mu j)^{1/2} \rfloor$ with the verbatim rule, however, restores the regularity. Note that the remaining parametrization stays the same. The rule of equation (5) can be cast into an analytic expression, too, by noting the pattern of deviations, in particular taking into account integer points on the continuous square root function. Assuming μ is an integer, these points share the general form $(x, y) = \mu(j^2, j)$. It turns out that, for the rule of equation (5) to hold true, these points can be taken as support for a continuous, piecewise linear substitution of the continuous, smooth square root function by a family of integer-parametrized lines (Fig. 11).

It happens that for every interval $[\mu j^2, \mu(j+1)^2]$ the segment of the line exhibiting the smallest slope connects the supporting points. Taking the floor function on these piecewise linear segments as baseline function

$$\beta_\mu(j) = \left\lfloor \min\left\{ \frac{1}{2n+1} j + \frac{\mu(n^2+n)}{2n+1} \right\}_{n=0}^{\lfloor j/\mu \rfloor} \right\rfloor \qquad (61)$$

restores the regularity of the twin structure, as, for instance, in

$$\beta_4(j) \Rightarrow 0, 1, 2, 3, 4, 4, 4, 5, 5, 5, 6, 6, 6, 7, 7, 7, 8, \ldots. \qquad (62)$$

Now, by the rule of equation (5), the meaning of a preferentially integer baseline parameter μ as a repeat period becomes obvious.

A11. Interpretation: the case for odd moduli

The CSCT models developed so far share a common feature in that their twin modulus m is always an even number. While odd moduli are not excluded by the mathematical rules of CSCTs, they are troublesome with respect to the stereochemistry of the CSCTs. Decorated CSCTs as illustrated in Fig. 1 are incompatible with odd moduli, since they cause a geometrical frustration between atoms located at the twin domain boundary following a spiral's full turn. Such a geometrical frustration cannot be resolved even by considering the presence of a screw dislocation, which would, in principle, allow for a recovery of the cyclic periodicity of the alternating twin domains after two full turns instead of one, yet also yield another geometrical frustration, now created between twin domains of alternating polarity along the dislocation axis. Accordingly, a spiral growth model that has been constructed based on the rhombic Penrose tiling (Baranidharan, 1990) does not take into account any atomic decoration of its tiles.

Apart from this the observed dichotomy of two series existing for τ_m, as described in the main part of this work, makes it seem advantageous to consider the fundamental twin modulus not being equal to m, but rather to $m' = m/2$ instead, for the following reasons: (i) if m' is taken to be of fundamental importance, the lower limit of $m' = 3$ becomes meaningful, since an equilateral triangle is the regular polygon with the smallest possible number of vertices; (ii) the classification into two series indexed by odd and even m' is emphasized; (iii) CSCTs for which m is an odd number are excluded, just by definition; (iv) if CSCTs are decorated with distinct atoms of alternating z coordinates, thereby forming alternating twin domains breaking the m-fold rotation symmetry, the number m' reflects the reduced order of the point group after the symmetry reduction. This makes m' appear to be the more natural parameter to consider.

Acknowledgements

The author thanks Peter Zeiner for his independent proof of equation (37), Peter Stampfli for giving the geometric explanation of equation (8), Walter Steurer for providing literature on the inflation factors of dodecagonal quasiperiodic tilings, and Michal Dušek for his endorsement.

Funding information

This work was supported by the Czech Science Foundation through research grant No. 18-10438S.

References

Adler, I., Barabe, D. & Jean, R. V. (1997). *Ann. Bot.* **80**, 231–244.
Andersson, S. (1983). *Angew. Chem. Int. Ed. Engl.* **22**, 69–81.
Andersson, S. & Hyde, B. G. (1982). *Z. Kristallogr.* **158**, 119–131.
Andersson, S. & Stenberg, L. (1982). *Z. Kristallogr.* **158**, 133–139.
Baranidharan, S. (1990). *Pramana – J. Phys.* **35**, L593–L598.
Borwein, J. M. & Borwein, P. B. (1987). *Pi and the AGM: a Study in Analytic Number Theory and Computational Complexity*, Section 3.7, pp. 91–101. New York: Wiley.
Borwein, J. M., Glasser, M. L., McPhedran, R. C., Wan, J. G. & Zucker, I. J. (2013). *Lattice Sums Then and Now.* Cambridge: Cambridge University Press.
Brown, K. (2018). *Non-Periodic Tilings With N-fold Symmetry*, https://www.mathpages.com/home/kmath539/kmath539.htm.
Burdik, Č., Frougny, Ch., Gazeau, J. P. & Krejcar, R. (1998). *J. Phys. A Math. Gen.* **31**, 6449–6472.
Bursill, L. A. (1990). *Int. J. Mod. Phys. B*, **04**, 2197–2216.
Bursill, L. A., Lin, F. J. & Fan, X. (1987). *Mod. Phys. Lett. B*, **01**, 195–206.
Chamizo, F. & Raboso, D. (2015). *Indagationes Math.* **26**, 723–735.
Davis, P. J. (1993). *Spirals – From Theodorus to Chaos.* Wellesley: A. K. Peters.
Dekking, F. M. & Mendèz France (1981). *J. Reine Angew. Math.* **329**, 143–153.
Deshouilliers, J.-M. (1985). In *Elementary and Analytic Theory of Numbers*, Banach Center Publications Vol. 17. Warsaw: PWN – Polish Scientific Publishers.
Dotera, T., Bekku, S. & Ziherl, P. (2017). *Nat. Mater.* **16**, 987–992.
Dotera, T., Oshiro, T. & Ziherl, P. (2014). *Nature*, **506**, 208–211.
Eagles, T. H. (1885). *Constructive Geometry of Plane Curves.* London: Macmillan.
Ericksen, J. L. (2006). *Math. Mech. Solids*, **11**, 3–22.
Fan, X., Bursill, L. A. & Peng, J. L. (1988). *Int. J. Mod. Phys. B*, **02**, 131–146.
Fan, X., Peng, J. L. & Bursill, L. A. (1988). *Int. J. Mod. Phys. B*, **02**, 121–129.
Feng, Z. Q., Yang, Y. Q., Huang, B., Li, M. H., Chen, Y. X. & Ru, J. G. (2014). *J. Alloys Compd.* **583**, 445–451.
Fontaine, A. & Hurley, S. (2006). *Forum Geom.* **6**, 97–101.
Frettlöh, D., Harriss, E. & Gähler, F. (2020). *Tilings Encyclopedia*, https://tilings.math.uni-bielefeld.de/.
Fullman, R. L. & Wood, D. L. (1954). *Acta Metall.* **2**, 188–193.
Graham, R. L., Knuth, D. L. & Patashnik, O. (1994). *Concrete Mathematics – a Foundation for Computer Science*, 2nd ed. New York: Addison–Wesley.
Grimmer, H. & Nespolo, M. (2006). *Z. Kristallogr.* **221**, 28–50.
Grünbaum, B. & Shephard, G. C. (1987). *Tilings and Patterns.* New York: W. H. Freeman and Company.
Hammer, Ø. (2016). *The Perfect Shape – Spiral Stories.* New York, Berlin, Heidelberg: Springer.
Hornfeck, W. (2012). *Acta Cryst.* A**68**, 167–180.
Hornfeck, W. (2018). *Acta Cryst.* A**74**, 659–672.
Hornfeck, W., Kobold, R., Kolbe, M., Conrad, M. & Herlach, D. (2018). *Nat. Commun.* **9**, 4054.
Hornfeck, W., Kobold, R., Kolbe, M. & Herlach, D. (2014). arXiv:1410.2952.
Hyde, B. G. & Andersson, S. (1989). *Inorganic Crystal Structures*. New York: John Wiley and Sons.
Hyde, B. G., Andersson, S., Bakker, M., Plug, C. M. & O'Keeffe, M. (1979). *Prog. Solid State Chem.* **12**, 273–327.
Jean, R. V. (1995). *Math. Biosci.* **127**, 181–206.
Jiang, W. J., Hei, K., Guo, Y. X. & Kuo, K. H. (1985). *Philos. Mag. A*, **52**, L53–L58.
Kunz, M. & Rothen, F. (1992). *J. Phys. I Fr.* **2**, 2131–2172.
Lawrence, J. D. (1972). *A Catalog of Special Plane Curves.* New York: Dover Publications.
Lehman, L. P., Xing, Y., Bieler, T. R. & Cotts, E. J. (2010). *Acta Mater.* **58**, 3546–3556.
Lehmer, D. H. & Lehmer, E. (1979). *Am. Math. Mon.* **86**, 725–733.
Lehmer, D. H. & Lehmer, E. (1980). *J. Reine Angew. Math.* **318**, 1–19.
Levitov, L. S. (1988). *Europhys. Lett.* **6**, 517–522.
Lockwood, E. H. (1961). *A Book of Curves.* Cambridge: Cambridge University Press.

Loxton, J. H. (1983). *Mathematika*, **30**, 153–163.
Müller, U. (2017). *Acta Cryst.* B**73**, 443–452.
Nakakura, J., Ziherl, P., Matsuzawa, J. & Dotera, T. (2019). *Nat. Commun.* **10**, 4235.
Nespolo, M. & Souvignier, B. (2015). *J. Mineral. Petrol. Sci.* **110**, 157–165.
Niizeki, K. (1989). *J. Phys. A Math. Gen.* **22**, 193–204.
Padrón-Navarta, J. A., Barou, F. & Daneu, N. (2020). *Acta Cryst.* B**76**, 875–883.
Pennybacker, M. F., Shipman, P. D. & Newell, A. C. (2015). *Physica D*, **306**, 48–81.
Plouffe, S. (1998). *Inverse Symbolic Calculator,* http://wayback.cecm.sfu.ca/projects/ISC/ and http://web.archive.org/web/20050812010306/http://pi.lacim.uqam.ca/Eng/.
Quiquandon, M., Gratias, D., Sirindil, A. & Portier, R. (2016). *Acta Cryst.* A**72**, 55–61.
Rivier, N. (1988). *Mod. Phys. Lett. B*, **02**, 953–960.
Rothen, F. & Koch, A.-J. (1989*a*). *J. Phys. Fr.* **50**, 1603–1621.
Rothen, F. & Koch, A.-J. (1989*b*). *J. Phys. Fr.* **50**, 633–657.
Rutter, J. W. (2000). *Geometry of Curves.* Boca Raton: Chapman & Hall/CRC.
Sadoc, J.-F., Rivier, N. & Charvolin, J. (2012). *Acta Cryst.* A**68**, 470–483.
Schaad, T. P. & Stampfli, P. (2021). arXiv:2102.06046.
Shahani, A. J. & Voorhees, P. W. (2016). *J. Mater. Res.* **31**, 2936–2947.
Shikin, E. V. (1995). *Handbook and Atlas of Curves.* Boca Raton: CRC Press.
Shubnikov, A. V. (1961). *Sov. Phys. Cryst.* **5**, 469–476.
Sirindil, A., Kobold, R., Mompiou, F., Lartigue-Korinek, S., Perriere, L., Patriarche, G., Quiquandon, M. & Gratias, D. (2018). *Acta Cryst.* A**74**, 647–658.
Sirindil, A., Quiquandon, M. & Gratias, D. (2017). *Acta Cryst.* A**73**, 427–437.
Sloane, N. J. A. (2018). Editor. *The On-Line Encyclopedia of Integer Sequences*, https://oeis.org/.
Stenberg, L. & Andersson, S. (1982). *Z. Kristallogr.* **158**, 205–212.
Steurer, W. & Deloudi, S. (2009). *Crystallography of Quasicrystals – Concepts, Methods and Structures*, Springer Series in Materials Science, p. 126. New York, Berlin, Heidelberg: Springer.
Vogel, H. (1979). *Math. Biosci.* **44**, 179–189.
Wang, J., Zhang, B., He, Z. B., Wu, B. & Ma, X. L. (2016). *Philos. Mag.* **96**, 2457–2467.
Watson, J. D. & Crick, F. H. C. (1953). *Nature*, **171**, 737–738.
Yates, R. C. (1974). *Curves and Their Properties.* Reston, Virginia, USA: The National Council of Teachers of Mathematics.
Zucker, I. J. (2017). *Symmetry*, **9**, 314.
Zwikker, C. (1963). *The Advanced Geometry of Plane Curves and Their Applications.* New York: Dover Publications.